The Planetary Science Journal, 6:28 (11pp), 2025 February https://doi.org/10.3847/PSJ/ad9de9

ORIGIN: Laser Desorption Ionization Mass Spectrometry of Nucleobases for In Situ Space Exploration

Nikita J. Boeren[1,2], Peter Keresztes Schmidt[1], Marek Tulej[1], Peter Wurz[1,2], and Andreas Riedo[1,2]
[1] Space Research and Planetary Sciences, Physics Institute, University of Bern, 3012 Bern, Switzerland; nikita.boeren@unibe.ch, andreas.riedo@unibe.ch
[2] NCCR PlanetS, University of Bern, 3012 Bern, Switzerland
Received 2024 July 12; revised 2024 December 2; accepted 2024 December 6; published 2025 January 30

Abstract

The ORganics Information Gathering INstrument (ORIGIN) is a space-prototype laser desorption ionization mass spectrometer designed to analyze molecular biosignatures. Nucleobases, fundamental components of nucleic acids, have been found in carbonaceous meteorites and in returned samples from the asteroid Ryugu, which suggest their extraterrestrial origin and possibly their significance in prebiotic chemistry and the RNA world hypothesis. Therefore, future space missions should be equipped for the in situ detection of nucleobases at relevant concentrations. This study investigated six nucleobases—adenine, cytosine, 5-methylcytosine, guanine, thymine, and uracil—using the ORIGIN setup. All six are readily detected and identified, with the mass spectra showing parent ions and minimal fragmentation. Mixture analyses illustrate the instrument's quantitative potential. The detection limit for adenine was 52 fmol mm^{-2}, and we show that sensitivity can be further improved by increasing detector voltage and sampling more positions. This study demonstrates ORIGIN's capability to detect nucleobases at trace abundance levels. The detection of nucleobases and other molecular biosignatures on other planetary objects might offer new insights into the origin of life on Earth and the possibility of discovering life beyond our planet.

Unified Astronomy Thesaurus concepts: Time-of-flight mass spectrometry (2222); Biosignatures (2018); Astrobiology (74); Pre-biotic astrochemistry (2079); Astrochemistry (75); Space vehicle instruments (1548)

1. Introduction

Several current and proposed space exploration missions are dedicated to finding molecular biosignatures aiming to find answers to the origin of life and potential existence of extraterrestrial life in our solar system and beyond. Molecular biosignatures can be large polymers with a very high complexity, such as nucleic acids, which strongly indicate the presence of life (M. Neveu et al. 2018). However, smaller and less complex molecules associated with life as we know it could also be potential indicators for extraterrestrial life, remnants thereof, or prebiotic life. Building blocks that are used by terrestrial life, such as amino acids, lipids, and nucleobases, are examples of such less complex biosignatures (J. Parnell et al. 2007; J. W. Aerts et al. 2014; K. P. Hand et al. 2017; M. Neveu et al. 2018; B. Cavalazzi & F. Westall 2019).

Nucleobases, also referred to as nitrogenous bases or nucleic acid bases, could act both as indicators of potential biotic activity and as essential components of the prebiotic chemistry that may have paved the way for life's origin (E. Camprubí et al. 2019; P. B. Rimmer and O. Shorttle 2019). Nucleobases are nitrogen heterocycles that form the fundamental constituents of the building blocks of nucleic acids, encoding the genetic information for protein formation. Cytosine (C), thymine (T), and uracil (U) are classified as pyrimidines with a single-ring structure, while adenine (A) and guanine (G) are purines with a two-ring structure. These informational monomers form canonical Watson–Crick base pairs in DNA, pairing G-C and A-T (with T exchanged for U in RNA; J. D. Watson and F. H. C. Crick 1953). These nucleobases are ubiquitously present in life on Earth and are considered an ancient feature of life (G. F. Joyce 2002; J. P. Dworkin et al. 2003).

In the 1970s, nucleobases, up to that point exclusively linked with terrestrial life, were discovered in carbonaceous meteorites, extending their presence beyond Earth (R. Hayatsu et al. 1975; P. G. Stoks and A. W. Schwartz 1979, 1981). Studies of meteorites, like Murchison, Murray, and Orgueil, have identified nucleobases, primarily adenine and guanine, along with other purines (R. Hayatsu et al. 1975; P. G. Stoks and A. W. Schwartz 1979, 1981; Z. Peeters et al. 2003; Z. Martins et al. 2008; M.P. Callahan et al. 2011; B. K. D. Pearce and R. E. Pudritz 2015; D. P. Glavin et al. 2018; Z. Martins 2018; Y. Oba et al. 2022). Recent work, first by Y. Oba et al. (2022) and later also by T. Koga et al. (2024), identified all five canonical bases, as well as other noncanonical purines and pyrimidines, at concentrations in the parts per billion (ppb) range in carbonaceous meteorites. Although such low concentrations might raise concerns regarding potential terrestrial contamination in the meteorites, a previous study regarding the carbon isotope ratios of certain nucleobases (uracil and xanthine, a noncanonical purine) indicated an extraterrestrial origin (Z. Martins et al. 2008). In addition, samples returned from the asteroid Ryugu by the JAXA Hayabusa2 spacecraft further imply the extraterrestrial existence of nucleobases. Uracil, among other interesting building blocks, has been identified in Ryugu samples and quantified in the low ppb range (J. C. Aponte et al. 2023; Y. Oba et al. 2023; E. T. Parker et al. 2023). Despite nucleobases exhibiting low stability in space owing to degradation by UV radiation (Z. Peeters et al. 2003; J. W. Aerts et al. 2014; H.J. Cleaves 2018), their detection in meteorites and on asteroid Ryugu strongly indicates the potential for their formation and persistence beyond Earth, potentially facilitated by sufficient protective conditions.

Table 1
Nucleobase Standards Used in This Study, Including Their Molecular Weight, Molecular Formula, and Purity (All Purchased from Sigma-Aldrich)

Compound	Molecular Weight (g mol^{-1})	Molecular Formula	Purity	Mixture Concentration (μmol l^{-1})			
				1	2	3	4
Adenine (A)	135.1	$C_5H_5N_5$	⩾99%	75	20	75	25
Cytosine (C)	111.1	$C_4H_5N_3O$	⩾99%	75	40	75	50
5-methylcytosine (mC) hydrochloride	161.6	$C_5H_7N_3O \cdot HCl$	⩾99%	75	60	25	125
Guanine (G)	151.1	$C_5H_5N_5O$	98%	75	80	25	25
Thymine (T)	126.1	$C_5H_6N_2O_2$	⩾99%	75	120	50	50
Uracil (U)	112.1	$C_4H_4N_2O_2$	⩾99%	75	140	50	125

Note. Concentrations for each nucleobase in the mixture standard solutions are provided in μmol l^{-1}. For each mixture solution, 1 μl was drop cast onto a sample holder, resulting in a surface concentration of ~10.6 pmol mm^{-2} for each compound in mixture 1 (75 μM), with surface concentrations in the same order of magnitude for the other mixtures.

The discovery of extraterrestrial nucleobases holds particular significance in the context of prebiotic chemistry and the RNA world hypothesis. The RNA world theory proposes that self-replicating RNA molecules preceded and catalyzed the emergence of proteins and DNA (W. Gilbert 1986). It is suggested that meteoritic impact could have delivered nucleobases to early Earth and other planetary objects, potentially reaching environments like warm little ponds where wet–dry cycles could aid polymerization (B. K. D. Pearce et al. 2017). Alternatively, nucleobases might have formed in situ in environments like warm ponds or at hydrothermal vents on the ocean bed, where all ingredients required for life (i.e., water, energy source, and chemical components) could be present (K. Kawamura 2004; L. E. Orgel 2004; B. T. Burcar et al. 2015; Y. Furukawa et al. 2015; L.E. Rodriguez et al. 2019).

The in situ detection of nucleobases on other planetary objects like Mars, Venus, Europa, or Enceladus could provide crucial information into the genesis and evolution of life on Earth (C. E. Carr et al. 2013; A. F. Davila and C. P. McKay 2014; M. Neveu et al. 2020; A. Davila 2021; S. Seager et al. 2023). Therefore, instrument payloads for future exploration missions should be capable of detecting and quantifying different nucleobases in extraterrestrial environments at trace-level abundances. This imperative is emphasized by various overviews, mission reports, and proposals, such as the ExoMars mission and the Europa Lander mission concept, where nucleobases are specifically listed as compounds of interest (J. Parnell et al. 2007; C. E. Carr et al. 2013; K. P. Hand et al. 2017; J. L. Vago et al. 2017; M. Neveu et al. 2018, 2020; B. Cavalazzi & F. Westall 2019; National Academies of Sciences, Engineering and Medicine 2022). Various experimental techniques capable of nucleobase detection have been described, including spectroscopic techniques, such as Raman spectroscopy, and mass spectrometric techniques, such as gas chromatography–mass spectrometry (GC-MS; W. Goetz et al. 2016; A.G. Moral et al. 2020; R. Bhartia et al. 2021).

Mass spectrometry instruments are in general favorable to be included in payloads owing to their detection sensitivity and capability to identify a wide array of compounds. The mass spectrometric instrument Mars Organic Molecule Analyzer (MOMA) on the ExoMars mission, with launch foreseen for 2028, is equipped to identify nucleobases, using derivatization necessary for pyrolysis GC-MS analyses, at concentrations below ppm levels with detection limits below nmol of analyte (J. L. Vago et al. 2017; Y. He et al. 2019). MOMA also incorporates a Laser Desorption Ionization (LDI)–MS component, which utilizes a laser to desorb and ionize larger nonvolatile organics (e.g., macromolecular carbonaceous compounds, proteins, and inorganic species), which will be the first LDI-MS instrument in space (J. L. Vago et al. 2017). A. Meneghin et al. (2022) recently provided a comparative analysis to correlate biosignatures to analytical techniques for a Mars sample return mission. Their study identified LDI-MS as a highly versatile and important technique for analyzing returned Martian samples, thereby illustrating the importance of LDI-MS for space exploration missions.

A different space-prototype LDI-MS instrument was developed at the University of Bern and is called the ORganics Information Gathering INstrument (ORIGIN). ORIGIN employs a pulsed UV laser for desorption and ionization of molecules and incorporates a reflectron-type time-of-flight (RTOF) mass analyzer. Previous studies using this instrument demonstrated the identification and quantification of amino acids, polycyclic aromatic hydrocarbons, and lipids at trace-level abundances (N. F. W. Ligterink et al. 2020; N. J. Boeren et al. 2022; K. A. Kipfer et al. 2022; P. Wurz et al. 2022). In this study, the measurement capabilities of nucleobases with ORIGIN will be discussed, including sensitivity improvements.

2. Materials and Methods

2.1. Sample Material and Preparation

Six nucleobase standards were investigated in this study, namely adenine (A), cytosine (C), 5-methylcytosine (mC), guanine (G), thymine (T), and uracil (U). See Table 1 for their molecular weight, formula, and purity, and see Figure 1 for the molecular structures. All standards and solvents were purchased at Sigma-Aldrich.

Stock solutions were prepared by dissolving nucleobase standards in MilliQ water (MilliPore, 18.2 MΩ·cm, <3 ppb total organic carbon). As guanine is insoluble in water, we opted for a different approach instead of acid addition, namely, to achieve a finely dispersed guanine solution in acetonitrile (HPLC grade, ⩾99.9%). Prior to usage, all guanine solutions were subjected to thorough sonication for optimal dispersion. Sample solutions were prepared by dilution of the stock solutions to the desired concentration with MilliQ water or acetonitrile (for guanine only). Both a water solution and acetonitrile solution without nucleobase standard were subjected to the same sample preparation steps and were considered as blank solutions. Sample solutions were prepared in a laminar flow bench (ISO 5) using high-purity

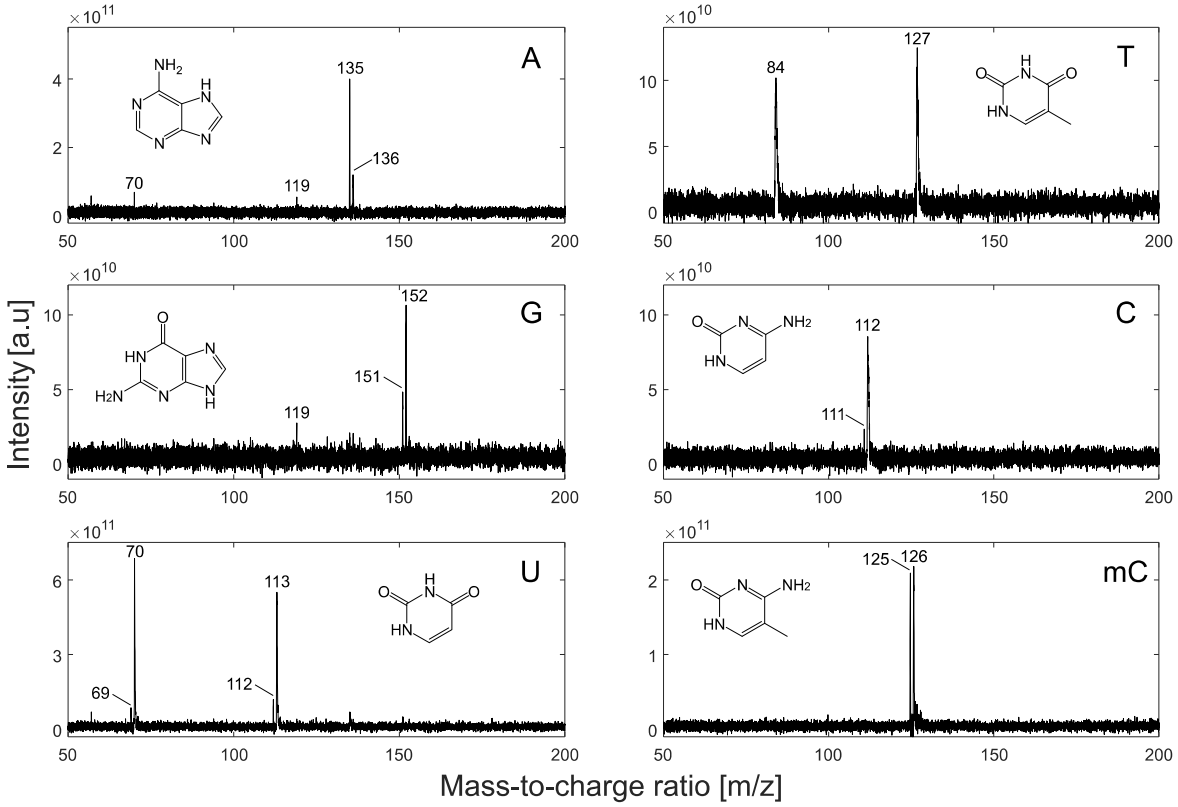

Figure 1. Mass spectra acquired by the ORIGIN setup of adenine (A), guanine (G), uracil (U), thymine (T), cytosine (C), and 5-methylcytosine (mC) with their molecular structure and peaks annotated by their corresponding *m/z* value. Concentrations were 5 pmol mm^{-2} for A; 14 pmol mm^{-2} for G, C, and mC; 707 pmol mm^{-2} for U; and 141 pmol mm^{-2} for T.

Eppendorf tubes and pipetting tips (both Biopur® grade), and all tools were flame sterilized before usage to avoid sample contamination.

Four mixture solutions were prepared by combining stock solutions in Eppendorf tubes and subsequently diluting them with water to achieve the desired concentrations. The concentrations of the nucleobases in the different mixtures are given in Table 1.

A stainless steel (1.4435) sample holder with 25 sample cavities (3 mm Ø with 0.2 mm depth) was used as the sample holder substrate. Before use, the holder was thoroughly cleaned by rinsing and sonication in a sequence of MilliQ water, isopropyl alcohol (cleaning grade), and again MilliQ water for 15 minutes each. Thereafter, the holder was put on a heating plate in a laminar flow bench for drying. Subsequently, the holder was argon ion sputtered (ion energies at 3 keV) for about 20 minutes under an angle of ∼20° in ultrahigh vacuum.

A sample solution was drop cast by pipetting 1 μl into a sample cavity. Afterward, the sample was left for solvent evaporation in a laminar flow bench for about 30 minutes. The sample holder with sample residue films in the cavities was subsequently placed into the vacuum chamber of ORIGIN for measurements. In addition, optical microscopy images (Zeiss Axiotech vario 100 HD, 5× magnification) were taken from high-concentration samples before placing them into the vacuum chamber to evaluate the residue distribution throughout the cavities.

2.2. The ORIGIN Setup

The ORIGIN setup is a space-prototype LDI-MS (N. F. W. Ligterink et al. 2020). A Q-switched Nd:YAG laser system (Quantel Brio) is utilized for sample desorption and ionization. The laser operates at a wavelength of 266 nm with a pulse width of approximately 3 ns at a 20 Hz laser pulse repetition rate. ORIGIN incorporates a miniature RTOF mass analyzer (160 mm × Ø 60 mm) for the separation of positively charged ions based on their time of flight (TOF), corresponding to their mass-to-charge ratio (*m/z*). The laser beam is guided through the central axis of the mass analyzer toward the sample surface.

Situated beneath the miniature mass analyzer, the sample holder is positioned on an X, Y, Z translation stage (Agilis, Newport). A multichannel plate (MCP) detector system in chevron configuration is located above the entrance of the mass analyzer (A. Riedo et al. 2017). The MCP detector generates an analog signal in response to incoming ions and was operated with a voltage over the detector of −1.7 kV (measured from top to bottom plate) unless stated otherwise. The signal is digitized by a high-speed analog-to-digital converter (U1084A, Agilent) with a selected sampling rate of 2 GS s^{-1}, resulting in TOF spectra lasting 20 μs. Further details about the instrument setup have been described previously (N. F. W. Ligterink et al. 2020).

2.3. Measurement Procedure

The vacuum chamber was vented using high-purity nitrogen (Carbagas, Alphagaz 2, N60) before introduction of the sample holder. Afterward, the holder was secured on the X, Y, Z translation stage below the mass analyzer. Subsequently, the chamber was evacuated to a pressure below 8×10^{-8} mbar for measurements within half a day or overnight.

Measurements were performed using an in-house standard protocol as has also been applied in previous studies

(N. F. W. Ligterink et al. 2020; N. J. Boeren et al. 2022; K. A. Kipfer et al. 2022). Laser pulse energies of 1.5–2.0 μJ were applied on the surface, which corresponds roughly to 75–100 MW cm^{-2}. We conducted a laser power scan on adenine to assess a suitable laser power for our study (see Appendix A).

A single measurement run consisted of sampling 40 individual positions, linearly spaced, in the sample cavity with approximately 50 μm distance (center to center). Per position, 100 laser shots were applied, resulting in a total of 4000 TOF spectra for each measurement. A raster scan of 30-by-30 positions was measured on a 7.1 mm^2 sample deposit of 5 pmol adenine ($\sim$700 fmol mm^{-2}) in a so-called "snake" pattern. At each position, 100 laser shots were fired, leading to a total of 90,000 mass spectra.

2.4. Data Analysis

A custom Matlab software suite was utilized for data analysis (S. Meyer et al. 2017). For each measurement, all spectra with peaks having a signal-to-noise ratio (SNR) $\geqslant 6$ among the 4000 spectra were coadded to generate a single TOF spectrum. A mass spectrum was calculated from the time spectrum by calibration using known mass peaks, such as Na^+ at *m/z* 23. In cases where not enough peaks were available for calibration, an average time value and constant value from several previous measurements were used for calculations. Simpson integration (of the time spectrum) was applied to each peak of interest by automatic integration window selection and background correction (S. Meyer et al. 2017). Peak identification was performed manually by comparison against blank measurements. Various peak characteristics were computed for peaks of interest, including peak area, SNR, and mass resolution ($m/\Delta m$). The limit of detection (LOD) of adenine was calculated by using the SNR of the 30-by-30 scan of $\sim$700 fmol mm^{-2} adenine. Details of the calculation can be found in Appendix B.

3. Results

Figure 1 displays the mass spectra of the six different nucleobases, while corresponding blank measurements are given in Appendix A. In nearly all cases, both the molecular ion $[M]^{\bullet+}$ and the protonated molecular ion $[M+H]^+$ were observed in the mass spectra. However, for thymine only the $[M+H]^+$ was observed at *m/z* 127. Notably, the ratio of $[M]^{\bullet+}$ and $[M+H]^+$ varied among the different compounds. For instance, adenine exhibited the parent ion $[M]^{\bullet+}$ as the dominant peak, whereas for uracil the parent peak was significantly lower compared to the protonated peak $[M+H]^+$. Minimal fragmentation was observed for all nucleobases, and there was negligible contamination or background from the sample holder substrate observed.

An extensive laser pulse energy scan was conducted on adenine and is given in Appendix A. The detection of adenine's molecular ion peak proved to be highly stable; across all tested laser pulse energies, the molecular ion remained detectable, and fragmentation was less pronounced at higher energies than expected. Notably, at approximately 5 μJ laser pulse energy, the laser ablation regime was already reached, evidenced by the appearance of elements in the mass spectra such as iron and titanium from the stainless steel substrate before significant fragmentation occurred.

In Figure 1, adenine and 5-methylcytosine exhibit notably high signal intensities, whereas cytosine is significantly lower. In our experimental setup, cytosine shows a significantly lower desorption and/or ionization efficiency as compared to 5-methylcytosine, despite the two molecules differing by only one methyl group. Uracil and thymine, both pyrimidines, demonstrate very low signal intensity. Their higher concentrations used in the measurements presented in Figure 1 are intended to show a representative spectrum. In the case of uracil, peaks at *m/z* 135 and *m/z* 151 are attributed to the alkaliated ions $[M+^{23}Na]^+$ and $[M+^{39}K]^+$, respectively. Additionally, the uracil measurement showed high sodium and potassium signals in the lower-mass region (see full range mass spectrum in Appendix A).

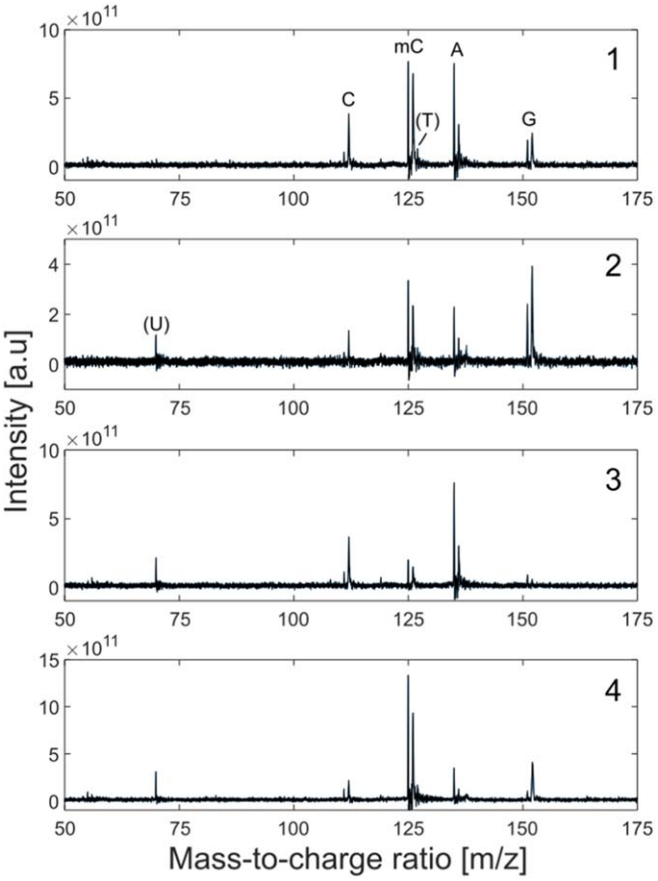

Figure 2. Mass spectra of four different mixtures of nucleobases adenine (A), guanine (G), cytosine (C), thymine (T), uracil (U), and 5-methylcytosine (mC), at various ratios acquired with ORIGIN. The ratios of the compounds in the mixtures can be found in Table 1.

At *m/z* 119, both adenine and guanine display a fragment peak in the mass spectrum, likely corresponding to the purine ring structure with all side chains fragmented off. Uracil shows a peak at *m/z* 70, which likely corresponds to the loss of −CONH that can occur at two possible locations. Similarly, thymine exhibits a peak at *m/z* 84, indicative for the loss of the same −CONH group, akin to the fragmentation of uracil, as they have the same ring structure. Notably, although cytosine and 5-methylcytosine could theoretically undergo the loss of −CONH at one position instead of two, no corresponding fragment peak was observed to indicate this.

3.1. Identification of Mixtures

Four different mixtures containing the six nucleobases at varying concentrations were analyzed. In Figure 2, the mass spectra of these mixtures are presented. Four nucleobases

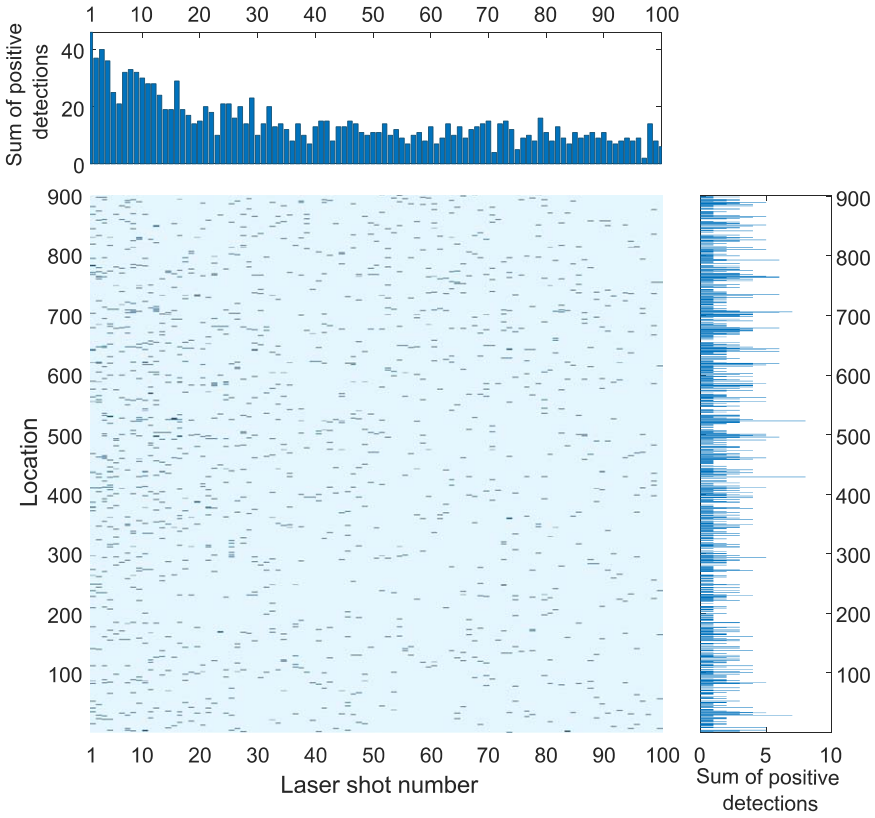

Figure 3. Distribution of positive detections of adenine at *m/z* 135 and 136 (SNR > 6) for 900 positions with 100 laser shots applied per position. Light blue: no detection; dark blue: positive detection. The histogram on top shows the adenine signal as a function of applied laser shots; the histogram on the right shows the adenine signal as a function of location in the sample cavity. The measurement was performed on a sample deposit of 5 pmol adenine spread out in a 7.1 mm^2 cavity.

(adenine, cytosine, 5-methylcytosine, and guanine) can readily be identified and are labeled in the upper mass spectrum. Thymine is potentially observed at a very low abundance around *m/z* 127, likely within the signal of 5-methylcytosine; however, the expected fragment peak at *m/z* 84, characteristic of thymine, is not detected. Uracil is challenging to detect in the spectra. The protonated molecular ion of uracil could not be definitively identified. However, the presence of a peak at *m/z* 70 may include a contribution from uracil.

The peak ratios vary significantly within and between measurements, as expected owing to the different concentrations of nucleobases in each mixture. In mixture 1, in which the nucleobases are present in equal concentrations, the variation in desorption and ionization efficiencies among the different compounds is clearly demonstrated. Notably, adenine and cytosine were present in the same absolute ratio in mixtures 1 and 3, as evidenced by their similar absolute intensity in mass spectra. Similarly, guanine and 5-methylcytosine maintained consistent ratios between mixtures 1 and 3, despite differences in their absolute concentrations. This is evident from the significantly lower absolute intensities of both peaks in mixture 3 compared to mixture 1, while the relative peak ratios between guanine and 5-methylcytosine remained constant.

3.2. Raster Scan and Sensitivity

A systematic raster campaign comprising a 30-by-30 grid of positions was conducted on a 7.1 mm^2 sample deposit of 5 pmol adenine, resulting in an approximate surface concentration of $\sim$700 fmol mm^{-2}. Figure 3 provides an overview plot illustrating positive detections of adenine for the 900 sampled positions and the 100 laser shots applied to each position. Positive detections, defined as spectra with peaks observed with an SNR exceeding 6σ for the molecular ion at *m/z* 135 and/or the protonated ion at *m/z* 136, are depicted in dark blue.

Adenine was consistently detected across the 900 positions, without a discernible specific spatial distribution, which means that there is a reasonable homogeneous film of the residue resulting from the evaporation of the solvent. However, certain positions exhibited no peaks for adenine, as expected for such a small sample spread over the sample cavity area. In addition, a subtle pattern in positive detections can be distinguished across the 100 laser bursts per position, as depicted in the top histogram. Initial measurements typically showed a slightly larger number of positive detections, followed by a gradual decrease with the increase of applied laser pulses on a position. Nevertheless, instances of a positive adenine detection were observed even for the final applied laser pulses at some locations, indicating that we did not exhaust the deposited sample material.

None of the positions yielded positive detections for all or even most laser shots, indicating limitations in sample material availability and/or insufficient energy for continuous desorption and ionization. The distribution plot illustrates a sufficient spread of the sample material in the sample cavity, and it also shows that there is still sample material left after sampling a certain number of positions with 100 laser shots per position. However, it is important to note that the LDI-MS technique is consuming the sample and that the finite size of a cavity or sample surface imposes physical constraints on the number of measurable locations.

Figure 4 depicts data from the same 30-by-30 raster campaign of adenine, with the peak area of *m/z* 135 and *m/z* 136 summed

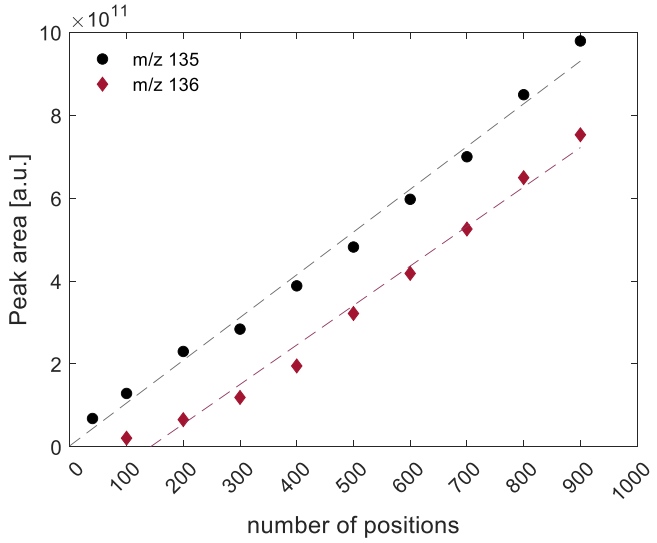

Figure 4. Peak areas of adenine *m/z* 135 and 136 peaks summed over the number of positions (total 900 positions) from the same 30-by-30 raster campaign (Figure 3).

over the locations. It is evident that as the number of sampled locations increases, and thus the amount of sampled material increases, the signal also increases accordingly. Additionally, both the molecular ion (*m/z* 135) and protonated molecular ion (*m/z* 136) follow the same trend, indicating a similar and stable desorption and ionization mechanism over all positions.

In this measurement, the surface concentration of adenine was 700 fmol mm^{-2}. The LOD (LOD$_{3\sigma}$) of 52 fmol mm^{-2} was calculated based on the SNR, with a detailed explanation provided in Appendix B. However, increased sensitivity is not solely achieved by sampling more locations; it can also be improved by increasing the voltage applied over the MCP stack. This effect is demonstrated through measurements of the same sample (700 fmol mm^{-2} adenine on 40 positions) at three distinct voltage settings, as detailed in Appendix C. A sensitivity increase of approximately 1.5-fold was discerned by increasing the voltage by 50 V between the different measurements, aligning with previously anticipated expectations (A. Riedo et al. 2017).

3.3. Sample Distribution

Optical microscope evaluation of the residue in the sample cavity was conducted on dried sample films to assess the distribution of the sample within the cavities. Figure 5 presents three microscope images displaying sample films of adenine and uracil, each at significantly higher concentrations as is necessary for visual observation, and an empty cavity as a reference. It should be noted that sample films with surface concentrations below ∼14 pmol mm^{-2}, derived from a 100 μM solution or lower, were too faint to be studied by an optical microscope.

Adenine, at a concentration of ∼140 pmol mm^{-2} from a 1 mM solution, appears to spread uniformly across the sample cavity, albeit with a visually lower density observed in the middle region, where measurements are typically conducted. This observation suggests a radial inhomogeneity of the sample material. Likewise, although uracil is not as clearly visible as adenine, uracil exhibits a lower sample density in the center and higher density along the edges of the cavity. Additionally, an empty location (visibly by eye) is observed in the right part of the cavity containing uracil, indicated by the arrow, possibly due to the presence of an air bubble during solvent evaporation.

4. Discussion

The detection capabilities of nucleobases using the ORIGIN space-prototype instrument were demonstrated in this study, which holds particular significance for future space missions aimed at identifying molecular biosignatures. Mass spectra revealed the presence of parent ions and/or protonated molecular ions for the measured nucleobases. Minimal fragmentation was observed even under laser pulses of higher power, and adduct formations were notably absent, except for uracil. This suggests a distinct desorption and ionization behavior for the nucleobases compared to previous studies on, e.g., lipids (N. J. Boeren et al. 2022). The mass spectra exhibited remarkably low background contamination, as evidenced by blank measurements included in Appendix A. Adjustments were made in the preparation of the sample holder for this study compared to prior studies involving argon ion sputtering, resulting in a significant reduction in contamination levels.

Differences in signal intensity among the different nucleobases were observed, as is consistent with expectations and previous measurements. Notably, there is a substantial difference in intensity between thymine and especially uracil compared to the other nucleobases. This suggests that purines are possibly more easily detected than pyrimidines. Possible explanations for the differences, such as laser-absorbance-related influences or sample distribution inhomogeneity, should be further explored.

The analysis of mixtures containing nucleobases at varying concentrations also clearly showed the differences in desorption and ionization efficiency between the different compounds. However, despite these different efficiencies, consistent ratios between nucleobases were observed. The changes in peak area ratios among different compounds correspond to the different concentration ratios. This shows the quantitative potential inherent in direct sampling and TOF analysis, where the number of ions reaching the detector is directly proportional to the peak area.

A typical mass resolution, $m/\Delta m$, of approximately 900 was achieved in the mass range of *m/z* 100–200 for the investigated mixtures of compounds. This mass resolution enables a clear distinction between cytosine and 5-methylcytosine, despite being chemically similar compounds differing only by a methyl group. This 15-unit mass difference holds particular significance for biologists, highlighting the importance of subtle molecular modifications in biological processes. However, spectral deconvolution will be necessary for more complex mixtures.

The LOD (LOD$_{3\sigma}$) for adenine was calculated based on the 30-by-30 position measurement (see Appendix B for details). The amount of the sample in the sample cavity was 5 pmol of adenine, corresponding to a surface concentration of ∼700 fmol mm^{-2}. The LOD$_{3\sigma}$ was determined from these measurements as 52 fmol mm^{-2}. This LOD aligns with mission requirements for nucleobase (and other organic molecule) measurements as defined for ExoMars with a requirement of LOD $\leqslant$ 1 pmol mm^{-2} (with SNR $\geqslant$ 3; F. Goesmann et al. 2017) and in the Europa Lander mission report with a requirement of LOD $\leqslant$ 141 fmol mm^{-2} (K.P. Hand et al. 2017).

There are several steps with which we can easily increase the sensitivity of ORIGIN, including adjusting the voltage applied over the MCP stack (Appendix C). Already an increase of 50 V on

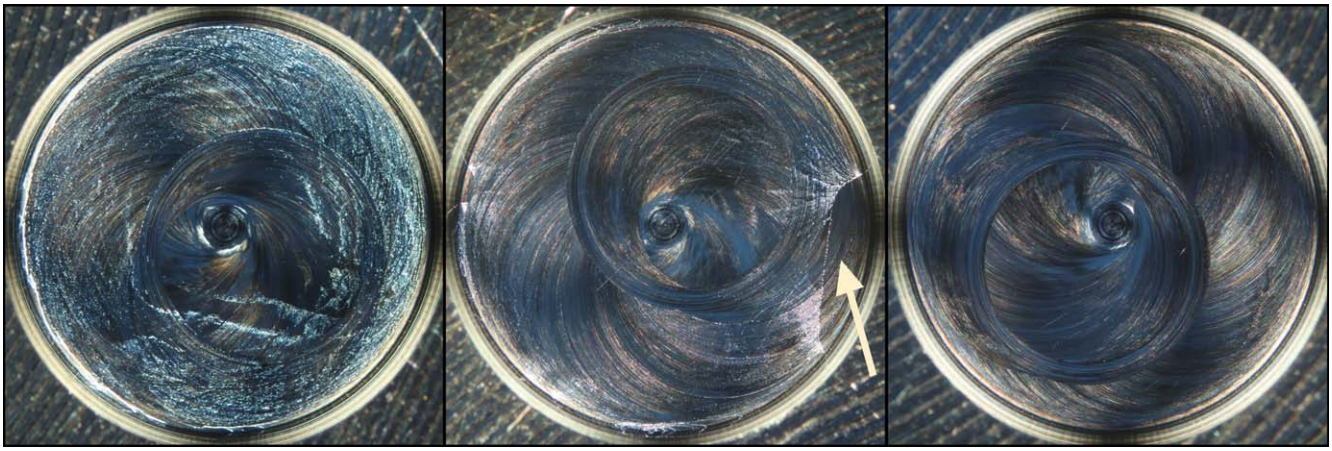

Figure 5. Optical microscopy images of sample cavities (Ø 3 mm) with adenine (left; ∼140 pmol mm^{-2}), uracil (middle; ∼140 pmol mm^{-2}), and an empty cavity (right).

the MCP detector voltage resulted in a signal increase by a factor of 1.5, aligning with previous expectations (A. Riedo et al. 2017), while the detector voltage still has a substantial reserve for further increase. Sampling more positions also led to a significant increase in the signal intensity of adenine, which can be expanded given that the sample material is not exhausted during the presented measurements (see Figure 4). Not all instruments can benefit from simply sampling more and thereby increasing sensitivity, but direct sampling and smaller laser impact areas allow for the measurement of additional locations. Nonetheless, constraints like sample availability and physical limitations of the sample holder and other payload restrictions, such as energy availability for laser operation, may impose limitations. Additionally, our sample handling approach offers the potential to concentrate samples within a cavity using a stepwise drop and evaporation process, a method that will be explored in future studies.

Optical microscope evaluation of high-concentration sample films provided insights into the spatial distribution of nucleobases within the sample holder cavities. If the observed spatial inhomogeneity for a high-concentration sample holds also for nominal concentrations, there is the potential for empty measurements at some locations and possibly a risk of undersampling. However, in the extensive 30-by-30 position scan, no specific local distribution of the sample was observed, and the sample film appeared to be spread out sufficiently uniform, albeit with typical variations as can be expected from drop casting (Figure 3). To improve quantification of the compounds in the sample, minimizing concentration gradients on the surface will be necessary by creating a uniform sample film if possible. One potential approach could involve heating of the holder during sample drop casting to facilitate direct solvent evaporation.

In this study, each measured position was subjected to 100 laser shots. It was observed (see Figure 3) that this extensive sampling might be redundant, as not all 100 shots per location yielded signal detections. The top histogram in Figure 3 reveals that more detections occurred in the earlier stages of the 100-shot sequence. This indicates that material is desorbed (and thus removed from the surface) with each applied laser pulse, meaning that less material is available on the surface with each applied pulse. However, material was detected throughout all 100 applied pulses, even toward the end of the 100-pulse sequence. This finding suggests a potential trade-off between increased sensitivity and energy saving and runtime on a mission, which would require a mitigation strategy to maximize sensitivity while keeping constraints in mind.

5. Conclusion and Future Perspective

This work demonstrates the capabilities of laser desorption and ionization mass spectrometry using the ORIGIN space-prototype instrument to detect nucleobases reliably at picomole levels. Although this detection sensitivity is already high, it can be enhanced through several methods, such as increasing the number of sampled locations, adjusting the voltage applied over the MCP detector, or employing sample concentration techniques. Although life elsewhere might utilize noncanonical nucleobases, we are confident that they can still be detected using the ORIGIN instrument, given the range of biomolecules that have been detected successfully so far. The detection of nucleobases and other molecular biosignatures on other planetary objects would offer potential insights into the origin of life and potential life beyond Earth.

Currently, ORIGIN is still a space prototype, and thus further work is required to reach flight readiness. Future development is focused on minimizing the optical footprint of the setup by integrating a microchip laser system. Furthermore, the mass analyzer and electronics will be tested within the framework of NASA's Artemis program under the Commercial Lunar Payload Services (CLPS) mission initiative, raising their overall readiness level (P. Keresztes Schmidt et al. 2022, 2024; P. Wurz et al. 2023). Future studies should also include extending the spectral library, conducting analyses on natural samples, and exploring collaboration and integration between instrumentation and sample collection and distribution methods.

Acknowledgments

The authors acknowledge the financial support of the Swiss National Science Foundation (SNSF) under grant 200020_207409. This work has been carried out within the framework of the NCCR PlanetS supported by the SNSF under grants 51NF40_182901 and 51NF40_205606.

Appendix A
Additional Mass Spectra

Additional mass spectra are given in this section. Figure A1 shows a laser pulse energy scan of adenine at low pulse energies. From this, it was determined that pulse energies of 1.5–2.0 μJ are preferred. A laser pulse energy scan of higher pulse energies can be found in Figure A2. This plot shows that fragmentation at

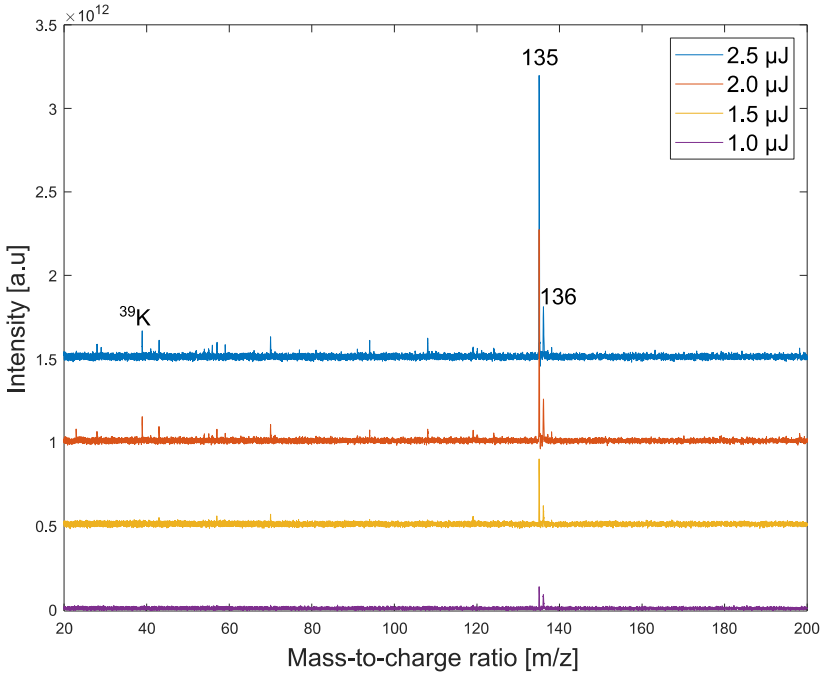

Figure A1. Laser pulse energy scan of adenine at a concentration of 7 pmol mm^{-2} with applied pulse energies of 1.0, 1.5, 2.0, and 2.5 μJ. Mass spectra are presented with an offset on the *y*-axis. By increasing the pulse energy, higher signals for adenine are observed at *m/z* 135 and 136, but also the background signals are increased. A pulse energy of 1.5–2.0 μJ was selected as optimal for the other measurements.

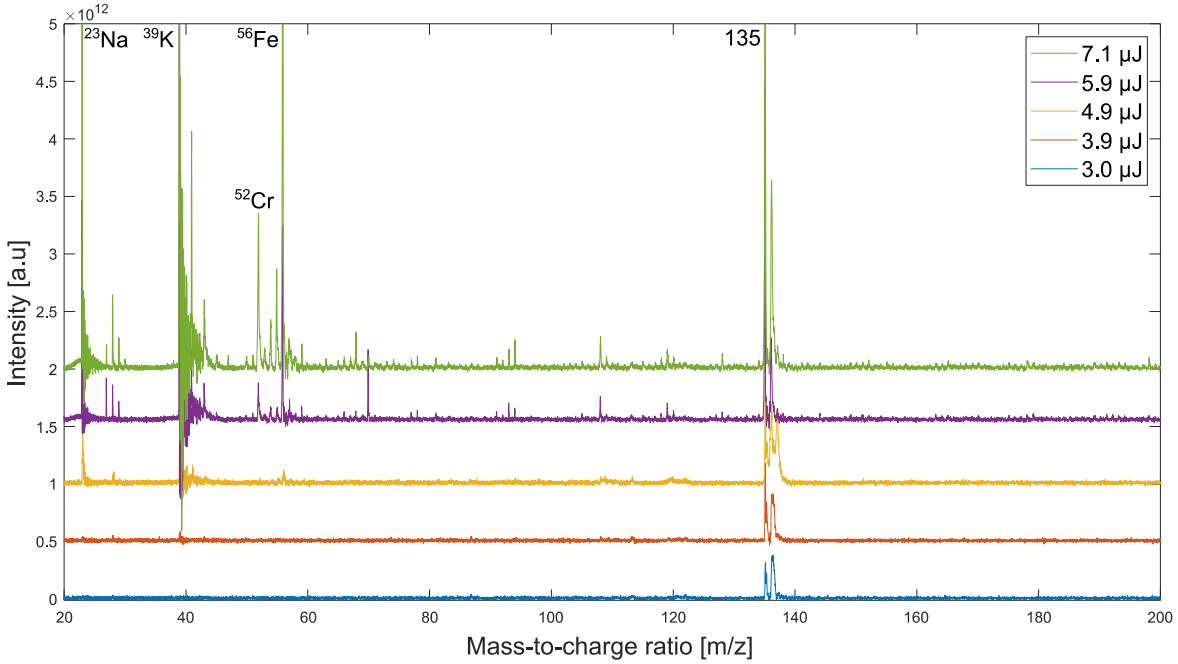

Figure A2. Laser pulse energy scan of adenine at a concentration of 14 pmol mm^{-2} with applied pulse energies of 3.0, 3.9, 4.9, 5.9, and 7.1 μJ. Mass spectra are presented with an offset on the *y*-axis. At 4.9 μJ, a peak at *m/z* 56 becomes visible, which can be assigned to ^{56}Fe from the stainless steel sample holder. This means that at this pulse energy the ablation regime is already starting, which can also be observed from the ^{23}Na and ^{39}K signals. Fragmentation of adenine is occurring as well, but it is not as severe as expected.

higher pulse energies is occurring but is less severe than expected. In addition, very high sodium and potassium signals are observed at higher pulse energies. At 4.9 μJ a peak at *m/z* 56, likely iron, is starting to appear. This can be attributed to iron from the stainless steel sample holder. Therefore, it was determined that these higher pulse energies mark the transition to the ablation regime. Mass spectra of blank measurements of the stainless steel sample holder, and of potential residue of MilliQ water and acetonitrile are displayed in Figure A3.

In Figure A4, the two mass spectra of Figure 1 of thymine and uracil are shown with the full measured *m/z* range. It can be observed that in the uracil measurement the signals for sodium

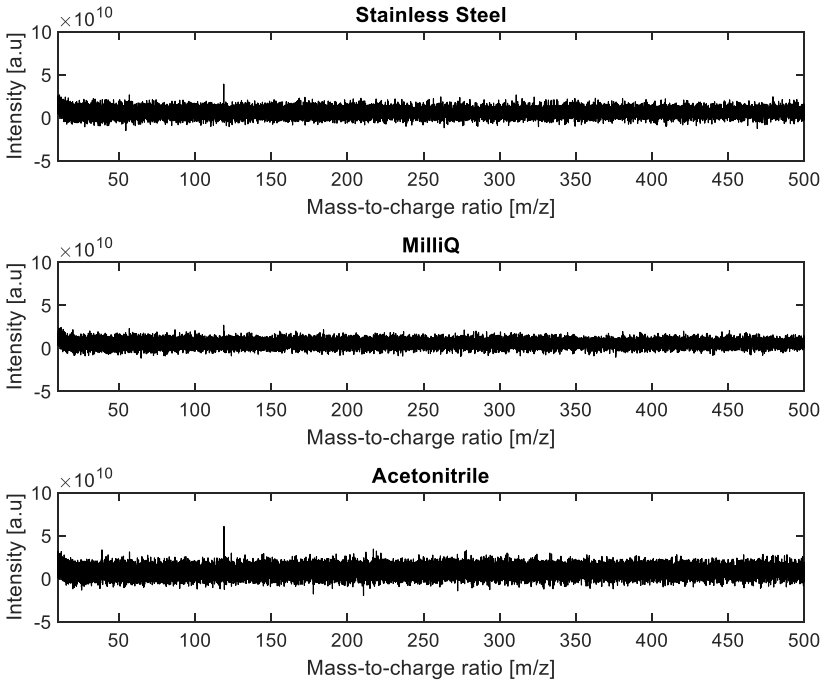

Figure A3. Mass spectra of three blank measurements of the stainless steel sample holder (top), MilliQ water (middle), and acetonitrile (bottom). Note that the solvents were evaporated prior to measurement, and these blank measurements are aimed at assessing potential residue left behind by the solvents.

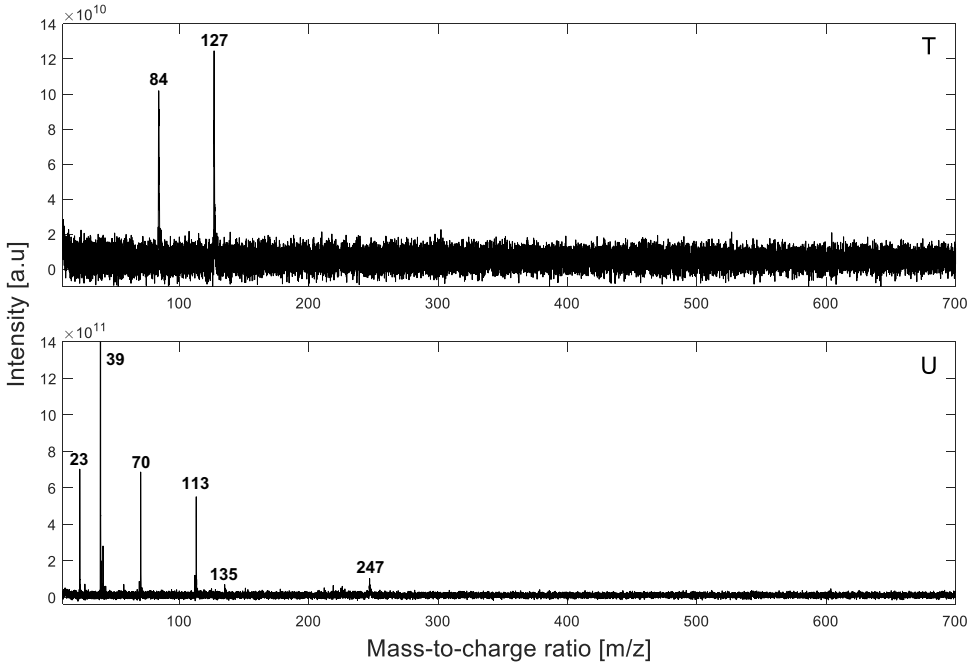

Figure A4. Mass spectra of thymine (T) and uracil (U) from Figure 1 with the complete measured *m/z* range with concentrations of 141 and 707 pmol mm^{-2}, respectively. Peaks are annotated with their corresponding *m/z* value.

(*m/z* 23) and potassium (*m/z* 39) are very high. This corresponds with the alkaliation that was observed for uracil. At *m/z* 135 a peak corresponding to $[M+23]^+$ is observed, and at *m/z* 151 a small $[M+39]^+$ peak can be seen.

Appendix B
Limit of Detection

In this study, the LOD is determined according to the method described by N. F. W. Ligterink et al. (2020), utilizing the average surface concentration (C_{surf}) and the SNR of a molecular ion peak. The LOD has been calculated for the 30-by-30 position scan from a 5 μM solution of adenine, of which 1 μl was pipetted into a cavity on the holder and the solvent was subsequently evaporated. This leaves 5 pmol spread out through the cavity with a surface area of 7.1 mm^2, which would (in the case of complete homogenous spreading) correspond to ~700 fmol mm^{-2}. By selecting 3σ as the limit for detection, the LOD is expressed as follows: $LOD_{3\sigma} = (3/SNR) \times C_{surf}$, with LOD and C_{surf} in fmol mm^{-2}. For the 700 fmol mm^{-2} adenine measurement, with an SNR of 40.8 for the peak at *m/z* 135, this gives

$LOD_{3\sigma} = 52$ fmol mm^{-2}. It needs to be noted that the LOD not only is compound dependent but also depends on the applied voltage on the detector, the number of sampled positions, and the applied laser pulse energy, among others. This measurement was performed on 900 positions, with a 2 μJ laser pulse energy on the surface and a voltage difference of 1752 V on the detector. All these factors can be further optimized, resulting in a higher SNR and thus lower LOD if needed.

To put this in context, the LOD requirement in the Europa Lander Science definition report is specified as 1 pmol material in a 1 g (~1 ml) water-ice sample (K. P. Hand et al. 2017). If we created a sample film from this in a cavity of 7.1 mm^2, this would translate to an LOD requirement of 141 fmol mm^{-2}. As also specified in the Europa Lander Report, the requirement would be 0.135 ppb by mass for adenine (135.1 g mol^{-1}) in 1 g of sample. In this case, our $LOD_{3\sigma}$ of 52 fmol mm^{-2} for adenine corresponds to 0.050 ppb by mass. Additionally, the LOD requirement for detection of these types of compounds by mass spectrometry for ExoMars is defined as below nmol analyte with an SNR above 10 (F. Goesmann et al. 2017).

Appendix C
Detector Voltage Scan

A detector voltage scan was performed on a 5 pmol deposit of adenine, which corresponds to ~700 fmol mm^{-2}, using three distinct voltage settings on the MCP detector. Figure C1 displays the peak area of *m/z* 135 (parent ion) corresponding to adenine for three different detector voltage settings. An increase in peak area of a factor 1.5 was observed with a voltage change of 50 V.

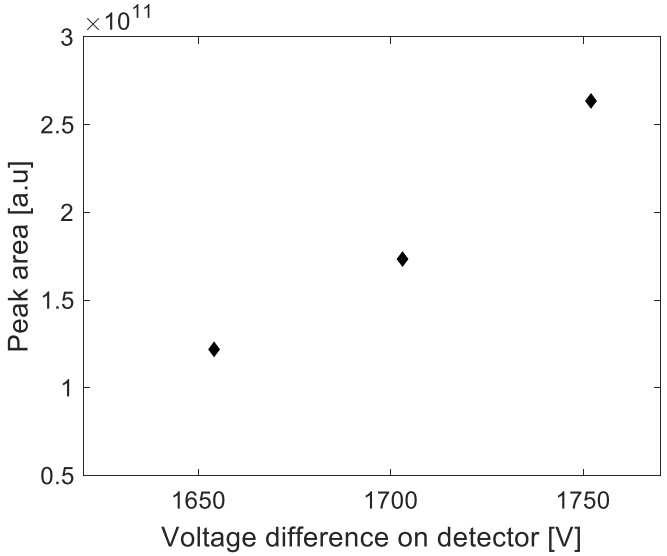

Figure C1. Detector voltage scan of the peak area of *m/z* 135 of adenine against the voltage difference on the MCP detector in V. A factor 1.5 signal increase is observed between the 50 V steps. The measurements were conducted on a 5 μM adenine sample (~700 fmol mm^{-2}) on 40 positions with a laser pulse energy of 1.5 μJ.

ORCID iDs

Nikita J. Boeren https://orcid.org/0000-0001-6162-6953
Peter Keresztes Schmidt https://orcid.org/0000-0002-4519-8861
Marek Tulej https://orcid.org/0000-0001-9823-6510
Peter Wurz https://orcid.org/0000-0002-2603-1169
Andreas Riedo https://orcid.org/0000-0001-9007-5791

References

Aerts, J. W., Röling, W. F. M., Elsaesser, A., & Ehrenfreund, P. 2014, Life, 4, 535
Aponte, J. C., Dworkin, J. P., Glavin, D. P., et al. 2023, EP&S, 75, 28
Bhartia, R., Beegle, L. W., DeFlores, L., et al. 2021, SSRv, 217, 58
Boeren, N. J., Gruchola, S., Koning, C. P. de, et al. 2022, PSJ, 3, 241
Burcar, B. T., Barge, L. M., Trail, D., et al. 2015, AsBio, 15, 509
Callahan, M. P., Smith, K. E., Cleaves, H. J., et al. 2011, PNAS, 108, 13995
Camprubí, E., de Leeuw, J. W., House, C. H., et al. 2019, SSRv, 215, 56
Carr, C. E., Zuber, M. T., & Ruvkun, G. 2013, in 2013 IEEE Aerospace Conf. Life Detection with the Enceladus Orbiting Sequence (Piscataway, NJ: IEEE), 11
Cavalazzi, B., & Westall, F. 2019, Biosignatures for Astrobiology, Advances in Astrobiology and Biogeophysics (1st ed.; Berlin: Springer)
Cleaves, H. J. 2018, in Prebiotic Chemistry and Chemical Evolution of Nucleic Acids, Nucleic Acids and Molecular Biology, ed. C. Menor-Salván (Berlin: Springer), 1
Davila, A. 2021, BAAS, 53, 034
Davila, A. F., & McKay, C. P. 2014, AsBio, 14, 534
Dworkin, J. P., Lazcano, A., & Miller, S. L. 2003, JThBi, 222, 127
Furukawa, Y., Nakazawa, H., Sekine, T., Kobayashi, T., & Kakegawa, T. 2015, E&PSL, 429, 216
Gilbert, W. 1986, Natur, 319, 618
Glavin, D. P., Alexander, C. M. O., Aponte, J. C., et al. 2018, The Origin and Evolution of Organic Matter in Carbonaceous Chondrites and Links to Their Parent Bodies, in Primitive Meteorites and Asteroids, ed. N. Abreu (Amsterdam: Elsevier), 205
Goesmann, F., Brinckerhoff, W. B., Raulin, F., et al. 2017, AsBio, 17, 655
Goetz, W., Brinckerhoff, W. B., Arevalo, R., et al. 2016, IJAsB, 15, 239
Hand, K. P., Murray, A. E., Brinckerhoff, W. B., et al. 2017, Report of the Europa Lander Science Definition Team 2016, Jet Propulsion Laboratory https://europa.nasa.gov/resources/58/europa-lander-study-2016-report
Hayatsu, R., Studier, M. H., Moore, L. P., & Anders, E. 1975, GeCoA, 39, 471
He, Y., Buch, A., Morisson, M., et al. 2019, Talan, 204, 802
Joyce, G. F. 2002, Natur, 418, 214
Kawamura, K. 2004, IJAsB, 3, 301
Keresztes Schmidt, P., Hayoz, S., Piazza, D., et al. 2024, in 2024 IEEE Aerospace Conf. Sample Handling Concept for In-situ Lunar Regolith Analysis by Laser-based Mass Spectrometry (Piscataway, NJ: IEEE), 11
Keresztes Schmidt, P., Riedo, A., & Wurz, P. 2022, CHIMIA, 76, 257
Kipfer, K. A., Ligterink, N. F. W., Bouwman, J., et al. 2022, PSJ, 3, 43
Koga, T., Takano, Y., Oba, Y., Naraoka, H., & Ohkouchi, N. 2024, GeCoA, 365, 253
Ligterink, N. F. W., Grimaudo, V., Moreno-García, P., et al. 2020, NatSR, 10, 9641
Martins, Z. 2018, Life, 8, 28
Martins, Z., Botta, O., Fogel, M. L., et al. 2008, E&PSL, 270, 130
Meneghin, A., Brucato, J. R., Fornaro, T., & Poggiali, G. 2022, IJAsB, 21, 287
Meyer, S., Riedo, A., Neuland, M. B., Tulej, M., & Wurz, P. 2017, JMSp, 52, 580
Moral, A. G., Rull, F., Maurice, S., et al. 2020, JRSp, 51, 1771
National Academies of Sciences, Engineering, and Medicine 2022, Origins, Worlds, Life: A Decadal Strategy for Planetary Science and Astrobiology (Washington, DC: The National Academies Press), 2023
Neveu, M., Anbar, A. D., Davila, A. F., et al. 2020, FrASS, 7, 26
Neveu, M., Hays, L. E., Voytek, M. A., New, M. H., & Schulte, M. D. 2018, AsBio, 18, 1375
Oba, Y., Koga, T., Takano, Y., et al. 2023, NatCo, 14, 1292
Oba, Y., Takano, Y., Furukawa, Y., et al. 2022, NatCo, 13, 2008
Orgel, L. E. 2004, Crit. Rev. Biochem. Mol. Biol., 39, 99
Parker, E. T., McLain, H. L., Glavin, D. P., et al. 2023, GeCoA, 347, 42
Parnell, J., Cullen, D., Sims, M. R., et al. 2007, AsBio, 7, 578
Pearce, B. K. D., & Pudritz, R. E. 2015, ApJ, 807, 85
Pearce, B. K. D., Pudritz, R. E., Semenov, D. A., & Henning, T. K. 2017, PNAS, 114, 11327
Peeters, Z., Botta, O., Charnley, S. B., Ruiterkamp, R., & Ehrenfreund, P. 2003, ApJ, 593, L129
Riedo, A., Tulej, M., Rohner, U., & Wurz, P. 2017, RSciI, 88, 045114
Rimmer, P. B., & Shorttle, O. 2019, Life, 9, 12
Rodriguez, L. E., House, C. H., Smith, K. E., Roberts, M. R., & Callahan, M. P. 2019, NatSR, 9, 9281

Seager, S., Petkowski, J. J., Seager, M. D., et al. 2023, PNAS, 120, e2220007120
Stoks, P. G., & Schwartz, A. W. 1979, Natur, 282, 709
Stoks, P. G., & Schwartz, A. W. 1981, GeCoA, 45, 563
Vago, J. L., Westall, F., Pasteur Instrument Team, et al. 2017, AsBio, 17, 471
Watson, J. D., & Crick, F. H. C. 1953, Natur, 171, 737
Wurz, P., Bandy, T., Mandli, P., et al. 2023, in 2023 IEEE Aerospace Conf. In Situ Lunar Regolith Analysis by Laser-Bbased Mass Spectrometry (Piscataway, NJ: IEEE), 11
Wurz, P., Tulej, M., Lukmanov, R., et al. 2022, in 2022 IEEE Aerospace Conf. Identifying Biosignatures on Planetary Surfaces with Laser-based Mass Spectrometry (Piscataway, NJ: IEEE), 11